Jurnal Rekayasa Proses dan Industri Terapan
Volume. 4 Nomor. 2 Mei 2026
e-ISSN: 2988-084X; p-ISSN: 2988-0831, Hal. 13-28
DOI: https://doi.org/10.59061/repit.v4i2.1548
Tersedia: https://e-journal.poltek-kampar.ac.id/index.php/REPIT

Comparative Robustness Evaluation of Code 128 and QR Codes under Controlled Degradation

Muhammad Sobri Maulana[1*], Dwitia Pratiwi[2], Arditya Prayogi[3]
[1-2]RSAU Prof. dr. Abdulrachman Saleh, Jakarta, Indonesia
[3]UIN K.H. Abdurrahman Wahid Pekalongan, Indonesia
**Corresponding Author: muhammadsobrimaulana31@gmail.com*

Abstract. Barcode robustness is determined jointly by symbol configuration, image quality, degradation geometry, and decoder behavior. This study presents a reproducible matched computational benchmark comparing Code 128 and QR Code under Gaussian blur, synthetic low-light noise, glare, perspective and rotational distortion, and simulated physical damage. Twelve deterministic alphanumeric payloads were encoded in both formats and evaluated at five ordered severity levels with three generated replicates per cell, producing 1,800 decoding trials or 900 matched pairs using the same ZBar engine. QR Code achieved a higher overall correct-decoding rate than Code 128 (72.3% vs 68.8%; paired risk difference 3.56 percentage points, 95% CI 0.32 to 6.79; McNemar p=0.037). The difference increased under predefined severe conditions, while performance remained degradation-specific: QR Code was more tolerant of blur, low-light noise, and moderate geometric distortion, whereas Code 128 performed better under the tested glare and distributed-damage models. Two Code 128 misdecodes under extreme distortion illustrate the importance of treating false decoding separately from no-read outcomes. The principal contribution is a severity-dependent benchmark framework rather than a new decoding algorithm or a claim of universal symbology superiority. The findings apply to the tested software-generated configurations and require validation with printed labels, measured lighting, and physical scanners before operational deployment.

Keywords: Barcode Robustness; Code 128; Image Degradation; QR Code; Traceability.

1. INTRODUCTION

Automatic identification and data capture technologies have become foundational components of contemporary manufacturing, warehousing, healthcare logistics, retail, maintenance, and product traceability. Linear barcodes remain attractive because they are inexpensive, compact, familiar to operators, and rapidly decoded in controlled environments, whereas two-dimensional symbols such as QR Code can encode substantially richer information in a small area and can incorporate error-correction mechanisms. This distinction is becoming increasingly relevant as industrial identification moves from a product-number paradigm toward data-rich traceability. GS1's current 2D transition guidance explicitly anticipates broader use of two-dimensional barcodes at the point of sale and across supply chains, allowing identifiers to be coupled with attributes such as lot, batch, expiry date, serial number, and digital-link information (GS1, n.d.; GS1 US, n.d.). Consequently, the engineering question is no longer merely whether a barcode can be scanned, but whether the selected symbol remains reliably decodable when the physical and optical environment departs from ideal conditions. Standards already recognize that symbol performance depends on more than nominal barcode type. ISO/IEC 15415:2024 defines print-quality measurement attributes for two-dimensional symbols, including decode, symbol contrast, modulation, axial

Naskah Masuk: 23 Maret, 2026; Revisi: 16 April, 2026; Diterima: 28 Mei, 2026; Terbit: 31 Mei, 2026;

nonuniformity, grid nonuniformity, unused error correction, and fixed-pattern damage, whereas ISO/IEC 15416:2025 addresses quality evaluation of linear barcode symbols. QR Code itself is standardized in ISO/IEC 18004:2024, while Code 128 is specified under ISO/IEC 15417. These standards are important because a label that is visually recognizable to a human observer may still fail to decode after defocus blur, low contrast, reflection, perspective deformation, abrasion, occlusion, or poor printing. GS1 implementation guidance similarly emphasizes quiet zones, geometric integrity, contrast, scanner compatibility, and the possibility that excessive damage consumes the error-correction capacity of a 2D symbol (GS1, n.d.). Thus, robustness is best treated as a measurable reliability characteristic rather than as an assumed feature of a symbology. The present study develops a controlled computational experiment comparing Code 128 and QR Code using matched payloads, common decoder logic, and five explicitly parameterized degradation mechanisms. The primary objective is to quantify correct-decoding probability across ordered severity levels and identify degradation-specific failure boundaries. Secondary objectives are to compare a normalized robustness area-under-the-curve (AUC) index, characterize decoding latency, identify false-decoding events, and examine whether stronger QR error correction changes resilience under glare and simulated physical damage. The study's novelty lies in its reproducible matched benchmark structure: both symbol families are exposed to the same payload content, degradation class, severity, replicate index, and decoder. It does not propose a new decoder and does not seek to establish an intrinsically superior symbology. Instead, it tests how complete symbol configurations respond to controlled perturbations and provides an experimental framework that can later be extended to printed labels, industrial scanners, and ISO-compliant verifier measurements.

2. THEORITICAL REVIEW

Recent computer-vision research demonstrates that degraded barcode images are a nontrivial engineering problem. Studies have investigated out-of-focus restoration, adaptive deblurring, motion-blur recovery, deep-learning-based shadow and white-out removal, recurrent feature reasoning, generative restoration, and super-resolution reconstruction for unreadable QR images (Chen et al., 2021a, 2021b; Dong et al., 2024; Gu et al., 2024; Ishikawa et al., 2023; Sancar, 2025; Yi & Chen, 2024). Muallim et al. (2025) recently introduced a lightweight restoration model and dataset for damaged barcode and QR images in logistics applications, while Zhang et al. (2026) proposed a lightweight causal Mamba network for blurred QR restoration. Earlier work also demonstrated that blur-invariant geometric design

and explicit deblurring priors can improve the recoverability of 2D codes under difficult imaging conditions (Rioux et al., 2019; Xie & Tan, 2021; Xu et al., 2024; Zheng et al., 2023). Collectively, this literature confirms that scanning failures are not edge cases; they are recurring operational problems that have motivated a growing restoration research field. Despite this progress, much of the recent literature optimizes restoration algorithms for one code family or one degradation mechanism, making it difficult to infer the relative failure boundaries of a conventional linear barcode and a QR Code when both are subjected to the same controlled perturbations and decoded by the same engine. Comparative applied studies often report aggregate recognition performance, yet standardized multi-factor benchmarks spanning blur, low-light noise, glare, geometric distortion, and physical damage remain limited, particularly when outcomes include no-read events, false decodes, and latency. Zakaria (2025), for example, reported practical differences between QR and linear-barcode detection, while the broader restoration literature has concentrated predominantly on QR-specific recovery. The unresolved methodological gap is therefore not the absence of another decoding algorithm, but the absence of a transparent matched framework that maps severity-dependent failure across different symbol architectures. The present study addresses that gap while restricting inference to the tested computational configurations. The central hypothesis is deliberately nonabsolute: QR Code is expected to outperform Code 128 under degradation patterns where two-dimensional redundancy and error correction preserve sufficient structural information, but Code 128 may remain competitive or superior for some localized occlusion and reflection patterns because the impact of damage depends on symbol geometry, label scale, and where the disturbance intersects critical features. By testing this hypothesis, the study aims to contribute a reproducible benchmark framework that can be extended to printer-substrate combinations, industrial scanners, smartphone cameras, and ISO-compliant verifier measurements.

3. RESEARCH METHOD

Study Design and Experimental Unit

A controlled computational robustness experiment was conducted using paired symbol instances. Twelve deterministic alphanumeric payload identifiers were generated and each payload was encoded in two formats: Code 128 as the one-dimensional comparator and QR Code as the two-dimensional comparator. Payload content was held constant within each pair and was not treated as an experimental factor. For each code type, five degradation factors were evaluated at five ordered severity levels with three generated replicates per payload-factor-

severity cell. Stochastic low-light noise and physical-damage placement used successive pseudorandom draws under one fixed seed (20260820), allowing replicate images to differ while remaining reproducible; deterministic transformations used the same parameter setting for the corresponding replicate index. The main benchmark consequently comprised 12 payloads x 2 code types x 5 factors x 5 severity levels x 3 replicates = 1,800 decoding trials, forming 900 matched Code 128-QR comparisons. The experimental unit was one generated degraded image presented to the decoder, and matched pairs were defined by identical payload, factor, severity, and replicate index.

Symbol Generation and Decoder Configuration

Code 128 symbols were generated with ReportLab using automatic Code 128 encoding and checksum handling. QR symbols were generated with the Python qrcode library using error-correction level M. For the short alphanumeric payload format used in the benchmark, the QR encoder selected Version 1 symbols (21 x 21 modules). The identical payload string was supplied to both symbol generators. Each rendered symbol retained its native aspect ratio and symbol-specific geometry and was placed on a 600 x 400 pixel white canvas before degradation; the symbols were not stretched to identical module or bar widths. Decoding was performed with the same ZBar engine accessed through pyzbar version 0.1.9. A trial was classified as a correct decode only when the expected original payload was returned. A different returned payload was classified as a false decode or misdecode, while no returned payload was classified as a no-read. Decode latency was the elapsed decoder execution time in milliseconds. Because module size, narrow-bar width, occupied area, and aspect ratio differed by design, the study evaluates the complete generated configurations and does not estimate size-independent intrinsic performance of either symbology.

Degradation Models

Table 1. Experimental degradation matrix and severity parameterization.

Factor	Severity 0	Severity 1	Severity 2	Severity 3	Severity 4
Gaussian blur	sigma=0	sigma=0.5	sigma=0.9	sigma=1.3	sigma=1.8 px
Low-light + noise	1.00; SD 0	0.80; SD 2	0.62; SD 5	0.45; SD 8	0.30; SD 12
Glare band	none	8 px; alpha .45	18 px; alpha .65	35 px; alpha .82	60 px; alpha .96
Distortion	0; 0 deg	0.06; 4 deg	0.14; 9 deg	0.26; 16 deg	0.40; 25 deg
Physical damage	0%	0.5%	1.5%	3.5%	7.0%

Low-light entries show brightness multiplier and Gaussian-noise standard deviation. Distortion entries show perspective fraction and rotation. Physical damage percentages represent simulated occluded/scratched symbol area. Severity values are experiment-specific engineering parameters, not ISO barcode verifier grades. Five degradation mechanisms were

chosen to represent recurring optical, geometric, and physical failure classes in practical scanning. The five-level grids were designed as boundary-spanning engineering stress tests: severity 0 represented an undegraded reference, intermediate levels introduced progressively stronger perturbations, and severity 4 was intended to approach or reach the decoding-failure region for at least one configuration. The numerical levels were not converted from lux, viewing angle, modulation transfer, abrasion energy, or ISO verifier grades and should not be interpreted as calibrated field exposures. Gaussian blur progressively removed high-frequency bar and module edges. The low-light model reduced global brightness while adding Gaussian noise as a simplified representation of sensor uncertainty. Glare was represented by an increasingly wide, high-intensity diagonal band with greater opacity. Distortion combined perspective warping and rotation. Physical damage used randomly placed occlusion and scratch regions with total affected area increasing from 0% to 7% of the symbol region. These isolated computational models permit controlled severity-response comparison, but they do not reproduce a particular camera, printer, substrate, coating, lighting fixture, or damage process.

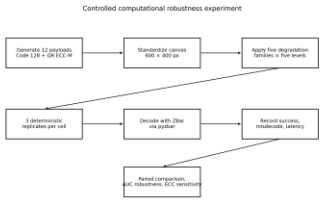


Figure 1. Workflow of the controlled matched-pair robustness experiment.

Source: controlled computational experiment conducted for this study (2026).

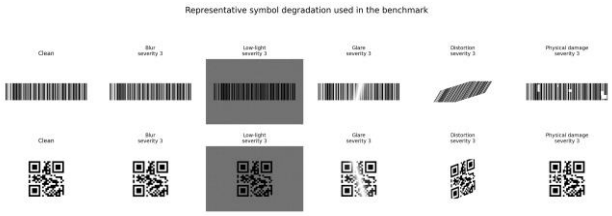


Figure 2. Representative Code 128 and QR Code images after severe computational degradation. Examples illustrate the visual form of the five perturbation classes rather than ISO verifier grades.

Source: controlled computational experiment conducted for this study (2026).

Outcomes and Statistical Analysis

The primary endpoint was correct-decode proportion at each factor-severity-code combination. Overall performance was summarized as the number and percentage of successful decodes. Because every Code 128 trial had a matched QR trial under the same payload, factor, severity, and replicate index, the prespecified primary comparison used the exact McNemar test on discordant pairs. The paired risk difference was calculated as QR

correct-decode probability minus Code 128 probability. Approximate 95% confidence intervals for the two headline paired risk differences were calculated from the matched-pair variance based on the discordant counts. A predefined secondary analysis included severity levels 3 and 4. Factor-by-severity McNemar tests were treated as exploratory diagnostics of failure boundaries; their p values were reported without multiplicity adjustment and were not interpreted as independent confirmatory claims. To summarize the complete severity trajectory, a normalized robustness AUC was calculated by trapezoidal integration over the ordered severity index scaled from 0 to 1. Because the physical spacing of severity parameters differed by factor, AUC comparisons were restricted to the two code types within the same factor. Decode latency was summarized descriptively by medians among successful scans because timing distributions were right-skewed. A separate sensitivity experiment compared QR error-correction levels M and H under glare and physical damage using eight payloads, five severity levels, and three replicates per cell.

4. RESULT AND DISCUSSION

Overall Decoding Performance

Table 2. Overall decoding performance and paired comparison.

Metric	Code 128	QR Code	Paired comparison
Decoding trials	900	900	900 matched pairs
Correct decodes	619 (68.8%)	651 (72.3%)	Risk difference +3.56 pp (95% CI +0.32 to +6.79)
Median decoder latency	2.94 ms	3.34 ms	Descriptive
False decodes	2 (0.22% of Code 128 trials)	0	2 events total
Exact McNemar test	–	–	p = 0.0372
Severe levels (3–4)	–	–	+11.94 pp (95% CI +5.32 to +18.56); p = 0.00064

Pp = percentage points. False-decode percentage shown in the Code 128 column uses 2/900 trials. Severe analysis includes severity levels 3 and 4 across all five degradation factors. Across the 1,800 main trials, QR Code produced 651 correct decodes from 900 attempts (72.3%), compared with 619/900 (68.8%) for Code 128. The absolute difference was modest when all severities, including the many easy clean or mildly degraded conditions, were pooled. However, the paired design revealed 127 instances in which QR succeeded while the matched Code 128 failed, compared with 95 instances in the opposite direction; 524 pairs were successful for both symbols and 154 failed for both. The exact McNemar test yielded p=0.0372, corresponding to a paired risk difference of +3.56 percentage points in favor of QR (95% CI +0.32 to +6.79). More importantly for reliability engineering, the difference became substantially larger when analysis was restricted to severity levels 3 and 4. In those 360

matched pairs, QR had 98 discordant wins versus 55 Code 128 wins, producing a +11.94 percentage-point advantage (95% CI +5.32 to +18.56) and p=0.00064. This divergence illustrates why average performance under mostly benign conditions can obscure the operational differences that become visible near a failure boundary.

Severity-Dependent Failure Boundaries

Table 3. Correct-decoding rate by degradation factor and severity.

Factor	Sev.	Parameter	Code 128 (%)	QR Code (%)
Blur	0	σ=0	100.0	100.0
	1	σ=0.5	100.0	100.0
	2	σ=0.9	100.0	100.0
	3	σ=1.3	83.3	100.0
	4	σ=1.8 px	0.0	100.0
Low-light	0	100%, noise 0	100.0	100.0
	1	80%, noise 2	100.0	100.0
	2	62%, noise 5	19.4	100.0
	3	45%, noise 8	0.0	100.0
	4	30%, noise 12	0.0	0.0
Glare	0	none	100.0	100.0
	1	8 px / α .45	100.0	91.7
	2	18 px / α .65	100.0	13.9
	3	35 px / α .82	0.0	0.0
	4	60 px / α .96	0.0	0.0
Distortion	0	none	100.0	100.0
	1	6% + 4°	100.0	100.0
	2	14% + 9°	100.0	100.0
	3	26% + 16°	16.7	61.1
	4	40% + 25°	0.0	0.0
Physical damage	0	0%	100.0	100.0
	1	0.5%	100.0	91.7
	2	1.5%	100.0	91.7
	3	3.5%	100.0	52.8
	4	7.0% symbol area	100.0	5.6

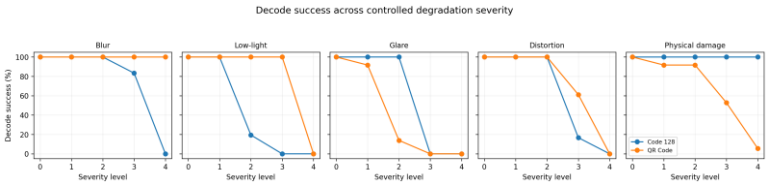


Figure 3. Correct-decoding probability across increasing degradation severity for Code 128 and QR Code.

Source: controlled computational experiment conducted for this study (2026).

The degradation curves show that the overall result was generated by markedly different failure mechanisms rather than by a uniform QR advantage. Under Gaussian blur, both symbols remained at 100% success through severity 2. At severity 3 (sigma=1.3), Code 128 fell to 83.3% while QR remained at 100%; at severity 4 (sigma=1.8 px), Code 128 fell to 0% whereas every QR trial still decoded correctly. This pattern is consistent with the engineering intuition that a two-dimensional symbol with structured finder patterns and error correction can preserve

decodability despite moderate edge spreading, provided that modules remain sufficiently distinguishable. It also aligns with the strong attention given to QR deblurring in recent image-restoration literature (Gu et al., 2024; Xu et al., 2024; Zhang et al., 2026). Nevertheless, this experiment does not imply that any QR Code will tolerate sigma=1.8 blur in physical use; tolerance depends on module size, optical resolution, code version, focus, and the resampling chain. Low-light degradation produced an even sharper separation. At severity 2, the brightness factor was reduced to 0.62 with additional Gaussian noise (SD=5), and Code 128 success dropped to 19.4%, whereas QR remained at 100%. At severity 3 (brightness 0.45, noise SD=8), Code 128 reached 0% while QR still decoded in all trials. At the most extreme level, however, both symbols failed completely. This result indicates that two-dimensional redundancy can postpone, but not eliminate, a signal-to-noise failure threshold. It is noteworthy that QR decoding under low light also incurred the largest latency in the benchmark: among successful trials, the median was approximately 16.11 ms for QR compared with 7.10 ms for Code 128. In other words, the decoder was often able to recover QR information from degraded images, but at a computational cost. In embedded or high-throughput scanning systems, robustness and processing latency therefore need to be considered jointly rather than as independent quality attributes.

The glare condition produced the opposite ranking. Both code types were fully readable without glare, but QR success declined to 91.7% at severity 1 and to only 13.9% at severity 2, while Code 128 remained at 100% through severity 2. At severity levels 3 and 4, both code families failed. This should not be interpreted as a general statement that linear barcodes are intrinsically more glare-resistant. The glare model used a diagonal saturated band; depending on its location, the band can erase QR finder, timing, alignment, or data modules while still leaving enough uninterrupted vertical bar transitions in a long linear symbol for the decoder to reconstruct Code 128. GS1 quality guidance explicitly notes the importance of contrast, fixed-pattern integrity, and damage to error-correction capacity. The result is therefore best interpreted geometrically: specular reflections interact with symbol architecture, and reflection placement may be as important as total reflected area. Perspective and rotational distortion showed a threshold-type response. Both symbols remained perfectly readable through severity 2. At severity 3, which combined a perspective fraction of 0.26 with 16 degrees of rotation, QR decoded 61.1% of images compared with 16.7% for Code 128. The paired comparison at this level yielded a +44.44 percentage-point risk difference in favor of QR. At the most extreme distortion level, both correct-decode rates reached 0%. These results support the role of two-dimensional position-detection structures in correcting moderate viewpoint changes but also

demonstrate a hard boundary beyond which geometric information becomes insufficient for the decoder. Research on egocentric, mobile, or motion-degraded QR recognition similarly treats camera viewpoint and geometry as first-class problems rather than incidental noise. The physical-damage model yielded the most counterintuitive result. Code 128 remained at 100% correct decoding even when randomly distributed simulated occlusion and scratches reached 7% of the symbol area, whereas QR declined from 91.7% at severity 1 and 2 to 52.8% at severity 3 and 5.6% at severity 4. This does not contradict the existence of QR error correction. Error correction protects against a limited amount and pattern of missing or corrupted codewords; damage that intersects finder patterns, timing structures, or concentrates errors in unfavorable locations can still defeat decoding. In the present random-damage generator, many Code 128 scars did not remove enough critical bar-space transitions across the full barcode height to prevent decoding. Conversely, the compact QR symbol exposed structurally important regions to distributed occlusion. A separate ECC-H sensitivity test, discussed below, materially improved QR damage tolerance, confirming that configuration choices can change the apparent ranking. This result is a useful warning against treating ‘QR has error correction’ as a universal guarantee of physical robustness.

Normalized Robustness Index

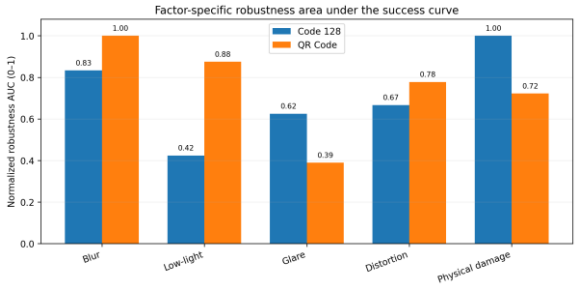


Figure 4. Normalized area under the success-versus-severity curve (robustness AUC) for each degradation factor.

Source: controlled computational experiment conducted for this study (2026).

Table 4. Factor-specific normalized robustness AUC.

Factor	Code 128	QR Code	Higher AUC
Blur	0.833	1.000	QR Code
Low-light	0.424	0.875	QR Code
Glare	0.625	0.389	Code 128
Distortion	0.667	0.778	QR Code
Physical damage	1.000	0.722	Code 128

The AUC analysis compresses each five-point degradation curve into a common 0-1 index and reinforces the factor-specific nature of performance. QR achieved an AUC of 1.000 under the tested blur range and 0.875 under low light, compared with 0.833 and 0.424 for Code 128. QR also exceeded Code 128 under distortion (0.778 vs 0.667), whereas Code 128 produced higher AUCs under glare (0.625 vs 0.389) and physical damage (1.000 vs 0.722). The index integrates over ordered severity rank rather than a calibrated physical dose; consequently, values support within-factor comparison between code types but should not be interpreted as directly comparable quantities across different degradation mechanisms. A single composite 'best barcode' claim would discard this interaction between symbol architecture and environment. Robustness AUC is not an ISO-defined quality score, but it provides a concise within-experiment summary of each severity-response profile.

Severe Conditions, Discordant Pairs, and Misdecoding

Table 5. Paired comparisons at severe degradation levels.

Factor	Severity	QR wins	Code 128 wins	Risk diff. (pp)	Exact p
Blur	3	6	0	+16.67	0.0312
Blur	4	36	0	+100.00	<0.0001
Low-light	3	36	0	+100.00	<0.0001
Low-light	4	0	0	0.00	1.0000
Glare	3	0	0	0.00	1.0000
Glare	4	0	0	0.00	1.0000
Distortion	3	20	4	+44.44	0.0015
Distortion	4	0	0	0.00	1.0000
Physical damage	3	0	17	−47.22	<0.0001
Physical damage	4	0	34	−94.44	<0.0001

A win means that one symbol decoded correctly while its matched counterpart failed. Zero discordant pairs occur when both symbol types uniformly succeed or uniformly fail. Risk difference is QR minus Code 128. Discordant-pair analysis makes the engineering trade-off especially clear near severe conditions. At blur severity 4 and low-light severity 3, QR won all 36 matched comparisons in which Code 128 failed, whereas at physical-damage severity 4 Code 128 won 34 of 36 pairs. Distortion severity 3 also favored QR, with 20 QR wins compared with four Code 128 wins. By contrast, extreme glare and the highest low-light and distortion settings sometimes created a region in which neither symbol remained usable, producing no discordant pairs and therefore no practical advantage for either format. This observation is

operationally important: a change in symbology cannot compensate indefinitely for inadequate optics, illumination, or label condition. Engineering controls that prevent entry into the 'both fail' region may yield greater reliability gains than simply switching from one barcode family to another. Two trials generated an outcome more consequential than a no-read: an incorrect payload was returned for Code 128 under distortion severity 4. In both cases, the expected alphanumeric payload was not recovered and the decoder instead returned the numeric string '555582'. The overall frequency was 2/1,800 trials (0.11%), or 2/900 within the Code 128 arm, but both events clustered in the most extreme distortion cell. The sample is far too small to estimate a universal false-decode probability, and the phenomenon requires replication with independent decoders and physical scanners. Nevertheless, its presence justifies treating misdecode as a distinct safety endpoint. In inventory, medication, maintenance, or recall workflows, a no-read normally triggers a retry, whereas a plausible but incorrect identifier can silently propagate into downstream records. Real deployments should therefore incorporate checksum/symbology validation, expected-format constraints, master-data verification, duplicate scanning logic, and, where applicable, GS1 application-identifier validation rather than accepting any decoder output as trustworthy.

Decoder Latency

Table 6. Median decode latency among successful scans by degradation factor.

Factor	Code 128 (ms)	QR Code (ms)	Difference (QR − Code 128)
Blur	2.862	3.313	+0.451
Low-light	7.097	16.110	+9.013
Glare	2.981	3.363	+0.382
Distortion	3.778	3.476	−0.302
Physical damage	2.841	3.253	+0.412

Latency differences were small under clean, blur, glare, and physical-damage conditions, with medians generally around three milliseconds. The notable exception was low light, where successful QR decoding had a median latency of 16.11 ms compared with 7.10 ms for Code 128. This increase is plausible because degraded two-dimensional images may require additional localization and decoding work before a valid payload is recovered. The benchmark measured only decoder execution on a single computing environment; it did not include image acquisition, autofocus, network transfer, user aiming time, or application-level validation. Consequently, these values are useful for within-experiment comparison but should not be interpreted as end-to-end industrial cycle times. A future hardware study should record scan-to-acknowledgment time on fixed scanners and smartphones and should relate latency distributions to throughput requirements and operator workload.

Sensitivity to QR Error-Correction Level

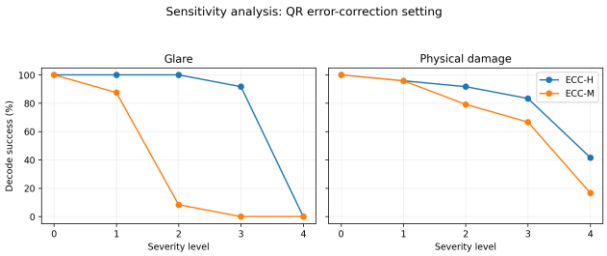


Figure 5. QR Code sensitivity analysis comparing error-correction levels M and H under glare and simulated physical damage (8 payloads; 3 replicates per cell).

Source: controlled computational experiment conducted for this study (2026).

Table 7. Selected severe-condition results from the QR error-correction sensitivity analysis.

Factor	Severity	ECC-M success (%)	ECC-H success (%)	Absolute gain (pp)
Glare	2	8.3	100.0	+91.7
Glare	3	0.0	91.7	+91.7
Glare	4	0.0	0.0	0.0
Physical damage	2	79.2	91.7	+12.5
Physical damage	3	66.7	83.3	+16.6
Physical damage	4	16.7	41.7	+25.0

The sensitivity experiment demonstrates that QR robustness is not a fixed property of the QR family. Increasing error correction from level M to H substantially shifted the failure curve in the tested glare model: at severity 2, ECC-H decoded 100% of trials while ECC-M decoded 8.3%, and at severity 3 ECC-H remained at 91.7% while ECC-M fell to 0%. At the most extreme glare level, both configurations failed, showing that stronger redundancy still has a finite limit. Under simulated physical damage, ECC-H also improved success from 16.7% to 41.7% at severity 4. These findings are directionally consistent with the QR standard's use of error-correction codewords and with GS1's warning that error-correction capacity can be consumed by damage. They also explain why comparisons between 'barcode' and 'QR' can be misleading unless QR version, module size, error-correction level, quiet zone, image scale, and decoder are explicitly reported. In practical deployment, ECC-H may be attractive for harsh environments, but its greater redundancy can increase symbol density or size for a fixed payload; therefore, the optimum must be established together with label-area constraints and scanner resolution. This comparison concerns the rendered ECC-M and ECC-H configurations produced by the stated generator; it should not be interpreted independently of QR version, module density, occupied area, and image scale.

Industrial Implications

For industrial and logistics engineering, the principal implication is that barcode choice should be framed as a reliability-design problem rather than a binary technology substitution. Organizations preparing for richer 2D data carriers should characterize the dominant failure

mechanisms at the actual point of use: defocus and motion in handheld scanning, low illumination in storage areas, specular glare on laminated packaging, oblique camera angles on conveyors, abrasion on reusable assets, or contamination in clinical and maintenance environments. A code that performs well against one mechanism can perform poorly against another. The present benchmark suggests that QR can create a substantial robustness margin for blur, low light, and moderate geometric distortion, whereas a linear Code 128 configuration can remain remarkably resilient under some distributed occlusion patterns. The appropriate engineering response is therefore to combine symbol selection with label-material selection, print-quality verification, lighting control, camera/scanner positioning, expected-format validation, and retry or exception workflows. For data-rich supply chains, GS1-compatible implementation should additionally ensure that identifiers, batch/lot, serial, expiry, and digital-link elements are parsed correctly rather than merely decoded as arbitrary text.

The results also provide a useful perspective on the transition toward 2D barcodes. The business value of 2D symbols often rests on additional information capacity and traceability, but operational value disappears if symbols cannot be decoded at production speed or after realistic degradation. Accordingly, migration programs should include an acceptance test matrix analogous to the framework used here: representative payloads, multiple label lots, defined severity classes, scanner diversity, false-decode monitoring, and paired performance against the incumbent 1D process. ISO/IEC 15415 and ISO/IEC 15416 verifier grades can complement such testing by providing standardized quality measures for printed symbols. A mature validation program should therefore distinguish three layers: conformance of the encoded data, physical print quality, and end-to-end operational decoding under realistic environmental stress. This layered approach is particularly important in safety-relevant contexts where the cost of a silent wrong identifier may exceed the cost of a temporary no-read.

Limitations and Future Validation

Several limitations constrain generalization and define the boundary of the study's claims. First, this was a computational image benchmark rather than a physical-scanner experiment; it did not model printer dot gain, substrate roughness, ink spread, lamination, spectral reflectance, autofocus, sensor demosaicing, rolling shutter, motion during exposure, or measured ambient-light geometry. Second, only one linear symbology, one primary QR error-correction level, one image canvas, one decoder engine, and a small set of short alphanumeric payloads were evaluated. Third, the severity levels were engineering parameters selected to span computational failure boundaries and cannot be equated with ISO/IEC 15415

or ISO/IEC 15416 verifier grades or with specific field exposures. Fourth, symbol dimensions, module widths, narrow-bar widths, and occupied areas differed between generated Code 128 and QR configurations; the results therefore compare complete configurations rather than intrinsic size-normalized symbologies. Fifth, the simulated damage distribution may favor or penalize particular geometries, so the Code 128 advantage under distributed damage requires replication using real abrasion, folding, liquid contamination, occlusion, and partial tearing. Sixth, the benchmark used repeated generated images within a limited payload set; reported inferential statistics describe the matched computational trials and do not substitute for population-level estimates across printers, scanners, labels, or operational sites. Future validation should use multiple printers, thermal-transfer and direct-thermal media, laminated and matte substrates, smartphone and fixed-mount scanners, measured lux and glare angles, conveyor motion, independent decoding libraries, and ISO-compliant verifier measurements.

5. CONCLUSION

This matched computational benchmark quantified the degradation-specific robustness of Code 128 and QR Code in 1,800 decoding trials forming 900 matched pairs. QR Code achieved a modestly higher overall correct-decode rate (72.3% vs 68.8%; paired difference 3.56 percentage points, 95% CI 0.32 to 6.79), and its advantage increased under the predefined severe-condition analysis. The global average nevertheless concealed strong interactions with degradation type: QR was more resilient to Gaussian blur, synthetic low-light noise, and moderate perspective and rotational distortion, while Code 128 performed better under the specific diagonal-glare and distributed-damage models. Two Code 128 misdecodes under extreme distortion further demonstrate why safety-oriented systems should distinguish misdecode from no-read. Increasing QR error correction from M to H shifted the tested glare and damage failure boundaries, confirming that configuration is an important design variable. The study contributes a reproducible severity-dependent comparison framework, not evidence that either symbology is universally superior. Operational selection should combine symbol configuration with print-quality verification, controlled optics and lighting, payload validation, and exception handling. Physical labels, multiple scanners and decoders, varied substrates, measured environmental conditions, and ISO/IEC 15415/15416 verifier grades are required before the numerical thresholds reported here can be generalized to industrial deployment.

ACKNOWLEDGEMENT

The authors declare no conflict of interest. This article reports a controlled computational experiment. All headline values, tables, and figures were calculated from 1,800 main decoding observations and a separate QR error-correction sensitivity dataset using a fixed random seed (20260820). The dataset represents computational experiments and must not be presented as measurements from physical scanners or printed labels.

REFERENCES

Chen, R., Yu, Y., Xu, X., Wang, L., Zhao, H., & Tan, H.-Z. (2021a). Fast restoration for out-of-focus blurred images of QR code with edge prior information via image sensing. *IEEE Sensors Journal, 21*, 18222–18236. https://doi.org/10.1109/JSEN.2021.3085568

Chen, R., Yu, Y., Xu, X., Wang, L., Zhao, H., & Tan, H.-Z. (2021b). Fast blind deblurring of QR code images based on adaptive scale control. *Mobile Networks and Applications, 26*, 2472–2487. https://doi.org/10.1007/s11036-021-01780-y

Dong, H., Liu, H., Li, M., Ren, F., & Xie, F. (2024). An algorithm for the recognition of motion-blurred QR codes based on generative adversarial networks and attention mechanisms. *International Journal of Computational Intelligence Systems, 17*, Article 450. https://doi.org/10.1007/s44196-024-00450-7

GS1 US. (n.d.). *What is GS1 Sunrise 2027?* Retrieved August 20, 2026, from https://www.gs1us.org/industries-and-insights/by-topic/sunrise-2027

GS1. (n.d.). *2D barcodes at retail point-of-sale implementation guidance*. Retrieved August 20, 2026, from https://ref.gs1.org/guidelines/2d-in-retail/

Gu, W., Sun, K., Jiang, Z., & Sun, L. (2024). Gs-DeblurGANv2: A QR code deblurring algorithm based on lightweight network structure. *Multimedia Systems, 30*, 87. https://doi.org/10.1007/s00530-024-01292-1

Ishikawa, Y., Okazaki, S., & Ohta, M. (2023). A method for removing shadows and white-outs on QR code images by deep learning. In *2023 IEEE 12th Global Conference on Consumer Electronics (GCCE)* (pp. 126–127). https://doi.org/10.1109/GCCE59613.2023.10315668

ISO/IEC. (2007). *ISO/IEC 15417:2007 Information technology Automatic identification and data capture techniques Code 128 bar code symbology specification*. International Organization for Standardization.

ISO/IEC. (2024a). *ISO/IEC 15415:2024 Information technology Automatic identification and data capture techniques Bar code symbol print quality test specification Two-dimensional symbols*. International Organization for Standardization.

ISO/IEC. (2024b). *ISO/IEC 18004:2024 Information technology Automatic identification and data capture techniques QR code bar code symbology specification*. International Organization for Standardization.

ISO/IEC. (2025). *ISO/IEC 15416:2025 Automatic identification and data capture techniques Bar code symbol print quality test specification Linear symbols*. International Organization for Standardization.

Latha, Y. M., & Rao, B. S. (2023). Advanced denoising model for QR code images using Hough transformation and convolutional neural networks. *Traitement du Signal, 40*, 1243–1249. https://doi.org/10.18280/ts.400342

Maulana, M. S., Pratiwi, D., & Prayogi, A. (2026a). MolecuTrace: Development of a web-based molecular oncology dashboard for integrating sample metadata, SNV profiles, and cancer stage classification. *Journal of Intelligent Systems and Information Technology, 3*(2).

Maulana, M. S., Pratiwi, D., & Prayogi, A. (2026b). Vaccination programs and infectious disease burden among military personnel: A systematic review with pathogen-specific quantitative synthesis. *The ASEAN Journal of Military and Preventive Medicine, 3*(2).

Muallim, T., Kucuk, H., Bareket, M., & Kahraman, M. (2025). Lightweight deep learning model and novel dataset for restoring damaged barcodes and QR codes in logistics applications. *Computer Modeling in Engineering & Sciences, 143*(3), 3557–3581. https://doi.org/10.32604/cmes.2025.064733

Rioux, G., Scarvelis, C., Choksi, R., Hoheisel, T., & Marechal, P. (2019). Blind deblurring of barcodes via Kullback-Leibler divergence. *IEEE Transactions on Pattern Analysis and Machine Intelligence, 43*, 77–88. https://doi.org/10.1109/TPAMI.2019.2927311

Sancar, Y. (2025). Reconstructing unreadable QR codes: A deep learning based super resolution strategy. *PeerJ Computer Science, 11*, e2841. https://doi.org/10.7717/peerj-cs.2841

Xie, S., & Tan, H.-Z. (2021). Blur-readable two-dimensional barcode based on blur-invariant shape and geometric features. *International Journal of Advanced Robotic Systems, 18*. https://doi.org/10.1177/1729881421999589

Xu, B., Jin, R., Li, J., Zhang, B., & Liu, K. (2024). Robust and fast QR code images deblurring via local maximum and minimum intensity prior. *The Visual Computer, 40*, 8809–8823. https://doi.org/10.1007/s00371-024-03272-y

Yi, J., & Chen, J. (2024). Enhancement of two-dimensional barcode restoration based on recurrent feature reasoning and structural fusion attention mechanism. *Electronics, 13*, 1873. https://doi.org/10.3390/electronics13101873

Zakaria, M. R. (2025). A comparative study on QR code and bar code detection techniques in modern systems. *International Journal of Synergy in Engineering and Technology, 6*(1), 14–22.

Zhang, H., Zhao, C., Jiang, S., Zhang, J., Zhang, J., & Chen, H. (2026). A lightweight causal Mamba network for blurred QR code image restoration. *Scientific Reports, 16*, 18932. https://doi.org/10.1038/s41598-026-49128-4

Zheng, H., Guo, Z., Liu, C., Li, X., Wang, T., & You, C. (2023). Blind deblurring of QR code using intensity and gradient prior of positioning patterns. *The Visual Computer, 40*, 441–455. https://doi.org/10.1007/s00371-023-02792-3